Gaining control of lipid-based nanomedicine by understanding the nano-bio interface

Pattipeiluhu, R.

Chapter 3

Anionic Lipid Nanoparticles Preferentially Deliver mRNA to the Hepatic Reticuloendothelial System

Lipid nanoparticles (LNPs) are the leading non-viral technology for the delivery of exogenous RNA to target cells in vivo. Such delivery platforms are exemplified by Onpattro®, an approved LNP-based RNA interference (RNAi) therapy, indicated for polyneuropathies resulting from transthyretin-mediated amyloidosis, administered systemically, and targeted to parenchymal liver cells. The discovery of systemically administered LNP technologies capable of preferential RNA delivery beyond hepatocytes has, however, proved more challenging. Here, preceded by comprehensive mechanistic understanding of nanoparticle biodistribution and clearance, we rationally design an LNP-based mRNA delivery platform to preferentially target the hepatic reticuloendothelial system (RES). Evaluated in embryonic zebrafish, validated in mice and compared to LNP-mRNA systems based on the lipid composition of Onpattro®, RES-targeted LNPs significantly enhance mRNA expression both globally within the liver and specifically within hepatic RES cell types. Hepatic RES targeting required just a single lipid change within the formulation of Onpattro® to switch LNP surface charge from neutral to anionic. This technology opens up new opportunities to treat liver-specific and systemic diseases in which RES cell types play a key role and highlights that rational development of advanced RNA therapies should be proceeded by a robust understanding of the nano-bio interactions involved.

This chapter was submitted as a research article: R. Pattipeiluhu, G. Arias-Alpizar, G. Basha, J. Bussmann, T.H. Sharp, M.A. Moradi, N. Sommerdijk, P.R. Cullis, A. Kros, D. Witzigmann, F. Campbell

3.1 Introduction

RNA therapy relies on cytosolic delivery of exogenous (therapeutic) RNA molecules, *e.g.* mRNA, siRNA, or miRNA, to gain precise control of gene expression within target cells.[1,2] This requires delivery systems to protect, transport and deliver highly charged, immunogenic and membrane impermeable RNA payloads within target cells and tissues in the body. To this end, lipid nanoparticles (LNPs) have emerged as the state-of-the-art, non-viral RNA delivery system for *in vivo* application.[3–5] These technologies are exemplified by Onpattro®, a clinically approved LNP-based RNA interference (RNAi) therapy, administered intravenously (*i.v.*) and used to treat polyneuropathies resulting from transthyretin-mediated amyloidosis (hATTR).[6,7] Onpattro® functions by transiently silencing transthyretin (TTR) expression specifically within hepatocytes through siRNA delivery.[7] Hepatocyte targeting is mediated through the adsorption of soluble apolipoprotein E (apoE) to the surface of a circulating LNP.[8,9] This, in turn, promotes LNP binding to the low density lipoprotein receptor (LDLr),[10] a receptor heavily expressed on the sinusoidal surface of hepatocytes. ApoE-LDLr binding leads to LNP endocytosis and consequent cytosolic siRNA delivery. Cytosolic siRNA release is enhanced by the protonation of ionizable (cationic) lipids within the endosome and subsequent disruption of the endosomal membrane.[11]

Following systemic administration, harnessing apoE-mediated LNP specificity for the delivery of RNA therapeutics (siRNA or mRNA) to hepatocytes is relatively common.[5,10,12–15] However, expanding the scope of LNP-based gene therapies to other hepatic cell types (or non-hepatic cells), to gain access to a greater diversity of disease states, has so far proved more challenging. To meet this challenge, high throughput empirical screening of DNA-barcoded LNPs has revealed formulations that preferentially target extra-hepatic tissues (*e.g.* bone marrow)[16] and cells (*e.g.* T-cells),[17] as well as individual hepatic (*e.g.* liver endothelial) cell types.[18,19] However, while these empirical discoveries have enriched our understanding of the structure-activity landscape of LNP technologies, they have not revealed the fundamental biological mechanisms underpinning LNP transport and preferential cellular uptake *in vivo*. Only this knowledge can enable the rational design of new LNP-based RNA therapies with target cell specificity.[5,20]

Besides hepatocytes (comprising ~80% liver volume), the liver is composed of non-parenchymal liver cells, including Kupffer cells (KCs) and liver sinusoidal endothelial cells (LSECs).[21] Hepatic blood vessels, or sinusoids, connecting the hepatic artery and portal vein to the central vein, are primarily composed of LSECs (~70%) and KCs (~20%).[22,23] Together these two cell types make up the hepatic reticuloendothelial system (RES) whose

primary role is to maintain blood homeostasis through the scavenging of macromolecular waste and pathogens from blood.[24,25] LSECs, in particular, are specialized scavenger endothelial cells (SECs) and have one of the highest endocytic activities of any cell type in the body.[26] These cells are responsible for the clearance of endogenous macromolecules, such as oxidized low-density lipoprotein and hyaluronic acid,[25,27,28] as well as blood borne pathogens.[29,30] In large part, LSEC clearance of macromolecular waste and pathogens is mediated through an array of scavenger receptors (*e.g.* Hyaluronan- and Stabilin-receptors), heavily expressed on the luminal membrane of LSECs.[31–33] As a therapeutic target, LSECs play a crucial role in liver homeostasis, regeneration following acute injury, and in the pathogenesis of various liver diseases, including cirrhosis and liver cancer.[26,34] Additionally, as antigen presenting cells, LSECs are key regulators of hepatic adaptive immunity and systemic immunotolerance, and are therefore promising immunotherapy targets.[35]

Guided by mechanistic understanding of the systemic clearance of *i.v.* administered anionic nanoparticles by hepatic RES cell types,[36] here, we rationally design anionic LNPs to preferentially target and transfect the hepatic RES, *i.e.* scavenger receptor LNPs (srLNPs). This required just a single lipid compositional change within the formulation of Onpattro®. Using the embryonic zebrafish (*Danio rerio*) as convenient, accurate and cost effective *in vivo* model,[37] we qualitatively describe LNP biodistribution, mRNA delivery and expression of an exogenous fluorescent protein *in vivo*, at cellular resolution and in real time, focusing particularly on relative LNP uptake and mRNA expression within SECs, macrophages and hepatocytes of the embryo. Furthermore, we confirm scavenger receptor, Stabilin-1 and -2, mediated uptake of anionic LNPs by SECs. Finally, we validate preferential LNP-mediated mRNA transfection of the hepatic RES in mice.

3.2 Results

Previously, we have shown that *i.v.* administered, anionic nanoparticles (ranging in size from 10-150 nm) are rapidly and extensively cleared from circulation by scavenging endothelial cells (SECs) within the posterior cardinal vein (PCV), caudal *hematopoietic tissue* (CHT) and caudal vein (CV) of a two day old zebrafish embryo.[36] In teleost fish (*i.e.* zebrafish), and other aquatic vertebrates, SECs are not located primarily in the liver (as for LSECs in mammals), but reside in various other organs including scavenging (venous) blood vessels.[38] Mechanistically, anionic nanoparticle recognition and uptake by SECs is mediated by the scavenger receptors, Stabilin-1 (*stab1*) and Stabilin-2 (*stab2*).[36] Stabilin-1 and -2 are strongly expressed by LSECs in the mammalian liver[39] and *i.v.* injection of anionic liposomes in 6-8 week old mice resulted in extensive nanoparticle uptake within these cell

types.[36] In addition to SECs, anionic nanoparticles are also scavenged by blood resident macrophages, both within the CHT of the embryonic zebrafish and within the mouse liver (*i.e.* within KCs).[36,40] All together, these observations indicate that the embryonic zebrafish can be used to qualitatively predict *in vivo* nanoparticle interactions with mammalian RES cell types.

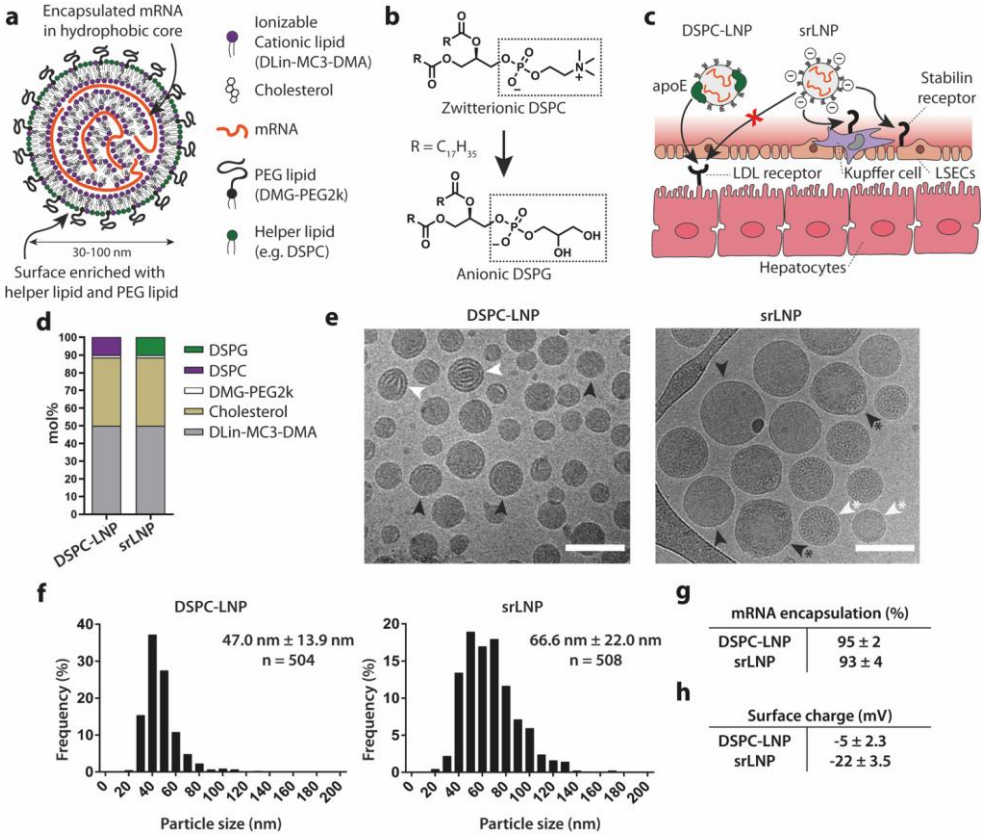

Figure 1. Design and characterization of srLNPs (**a**) Schematic of the structural organization of an LNP containing mRNA, as described previously.[41] Helper phospholipids (typically incorporated at 10 mol%) are enriched at the LNP surface. (**b,c**) Within the liver sinusoids, switching of the helper phospholipid from zwitterionic DSPC (as in ONPATTRO®) to anionic DSPG creates anionic srLNPs that are directed to the hepatic RES, *via* Stabilin receptor mediated recognition and uptake in LSECs. srLNP uptake within hepatic RES cells is further enhanced by the inhibition of apoE-LDLr interactions mediated by anionic phospholipids (*e.g.* DSPG).[42] The mechanism of recognition and uptake of srLNPs by blood resident macrophages (*i.e.* KCs) is not known. (**d**) Lipid composition of DSPC-LNPs (*i.e.* ONPATTRO®) and srLNPs. (**e**) Cryo-EM images of DSPC-LNPs and srLNPs (entrapping capped mRNA-eGFP) shows solid lipid nanoparticle structures. Scale bars: 100 nm.

Internal structures indicated with arrows: lamellar (white), amorphous (black), polymorphous (black*) and unilamellar (white*) (**f**) Size distribution of DSPC-LNPs and srLNPs, as determined by cryo-EM. The values derived from the frequency distribution graphs represent the mean ± s.d. (**g**) mRNA encapsulation efficiency within DSPC-LNPs and srLNPs, as determined by RiboGreen assay. (**h**) Surface charge of DSPC-LNPs and srLNPs, as determined by zeta potential measurements. See **Supporting Table 1** for full biophysical characterization of all formulations used in this study.

In this case, we rationally designed an anionic LNP system to enable preferential genetic manipulation in hepatic RES cells. In general, LNPs consist of five structural components (four lipid reagents and an oligonucleotide payload) that self-assemble to form discrete nanostructures ranging from ~30 to ~150 nm in size (**Figure 1a**).[43] The "hydrophobic" core of an LNP is rich in ionizable lipids (*e.g.* heptatriaconta-6,9,28,31-tetraen-19-yl 4-(dimethylamino) butanoate, DLin-MC3-DMA; 50 mol%)* [asterix denotes in the case of Onpattro®]), cholesterol (38.5 mol%)* and an oligonucleotide payload. The LNP surface (*i.e.* lipid-water interface), in contrast, is rich in helper phospholipids (*e.g.* 1,2-distearoyl-*sn*-glycero-3-phosphocholine, DSPC; 10 mol%)* and lipid-PEG conjugates (*e.g.* 1,2-dimyristoyl-rac-glycero-3-methoxypolyethylene glycol-2000, DMG-PEG2k; 1.5 mol%))*.[41] We therefore hypothesized that switching the helper phospholipid of Onpattro®, from zwitterionic DSPC to anionic 1,2-distearoyl-*sn*-glycero-3-phosphoglycerol (DSPG), would render an LNP surface anionic. In turn, an anionic surface charge would redirect LNP targeting and functional RNA delivery from hepatocytes to the hepatic RES by promoting Stabilin-mediated LNP recognition and uptake in LSECs whilst simultaneously inhibiting hepatocyte apoE-LDLr interactions (**Figure 1b,c**).[42] Hereafter, we refer to DSPG-containing LNPs as srLNPs and LNPs based on the lipid composition of Onpattro® as DSPC-LNPs (**Figure 1d**). In all cases, a nitrogen to phosphate (N:P) ratio of 6:1 was used, as is typical for larger nucleic acid payloads.[44]

Following microfluidic assembly, cryo-electron microscopy (cryo-EM) revealed LNPs with a typical electron-dense core structure (Figure 1e).[45–48] Within DSPC-LNPs (47.0 nm ± 13.9 nm), both amorphous and lamellar core structures were present, whereas the core structure of srLNPs (66.6 nm ± 22.0 nm) contained a mixture of amorphous, unilamellar and polymorphic structures, as has been previously reported for LNP-mRNA systems.[49,50] Particle sizes of both DSPC-LNPs and srLNPs (determined through cryo-EM image analysis) were comparable to the number-weighted average determined by dynamic light scattering (Figure 1f, Supporting Table 1) and, in all cases, mRNA encapsulation efficiencies were >95% (Figure 1g). Importantly, however, srLNPs possessed a significantly more anionic (ζ-potential ~ -20 mV) surface charge compared to DSPC-LNPs (ζ-potential ~ -5 mV), indicative of DSPG exposed at the lipid-water interface (Figure 1h). For detailed

biophysical characterization (*i.e.* size, surface charge, encapsulation efficiencies) of all formulations used in this study, please refer to Supporting Table 1.

To assess LNP biodistribution, DSPC-LNPs and srLNPs containing a fluorescent lipid probe (DOPE-LR, 0.2 mol%) and encaspulating fluorescently tagged mRNA (capped and Cy5-labelled), were injected (*i.v.*, ~10 mM lipid, ~0.2 mg/kg mRNA) in wildtype zebrafish embryos at two days post-fertilisation (dpf) (**Figure 2a**). Confocal imaging of entire live embryos, as well as high resolution, tissue level views to include key scavenging cell types of the embryo within the CV and CHT (**Figure 2b**), revealed distinct biodistribution patterns for both LNP-mRNA formulations at 1.5 hour post injection (hpi) (**Figure 2c-f**). In the case of DSPC-LNPs, particles were mostly freely circulating, with both lipid and mRNA confined to, and homogenously distributed throughout, the vasculature of the embryo (**Figure 2c,d**). In addition, a small fraction of DSPC-LNPs accumulated in blood-resident macrophages within the CHT of the embryo, indicative of low level recognition and uptake by the RES (white arrowheads, **Figure 2d**; confirmed in *mpeg*:mCherry embryos, **Figure S1a-c**). In the case of srLNPs, the majority of injected particles were cleared from circulation at 1.5 hpi, with highly selective accumulation observed within SECs and blood-resident macrophages within the PCV, CHT and CV of the two day old embryo (**Figure 2e,f**; macrophage uptake confirmed in *mpeg*:mCherry embryos, **Figure S1d-f**).

The selective accumulation of srLNPs within scavenging (venous) blood vessels of the embryonic zebrafish closely resembled previously observed biodistributions of anionic liposomes, polymersomes and inorganic nanoparticles, in which nanoparticle uptake within SECs was mediated by Stabilin scavenger receptors.[36] To confirm Stabilin-mediated uptake, srLNPs were injected (*i.v.*) in established *stab1*$^{-/-}$/*stab2*$^{-/-}$ double knockout (KO) zebrafish embryos (2 dpf).[51] Within these mutant embryos, srLNPs predominantly remained in circulation at 1.5 hpi with a small fraction accumulating within blood-resident macrophages of the CHT (**Figure 2g** and (whole embryo) **S2**). This confirmed that srLNPs selectively accumulate within RES cell types of the embryonic zebrafish and that recognition and uptake of srLNPs within SECs, but not macrophages, is mediated by Stabilin receptors. Analogous injections of DSPC-LNPs within double KO embryos did not alter DSPC-LNP biodistribution, with the majority of DSPC-LNPs remaining in circulation (**Figure 2h**, (whole embryo) **S2**). In all cases, both lipid and mRNA fluorescent probes appear fully colocalized at 1.5 hpi, suggesting mRNA remains stably entrapped within the core of both DSPC- and srLNPs in circulation, as well as during cellular recognition and (early) cellular uptake.

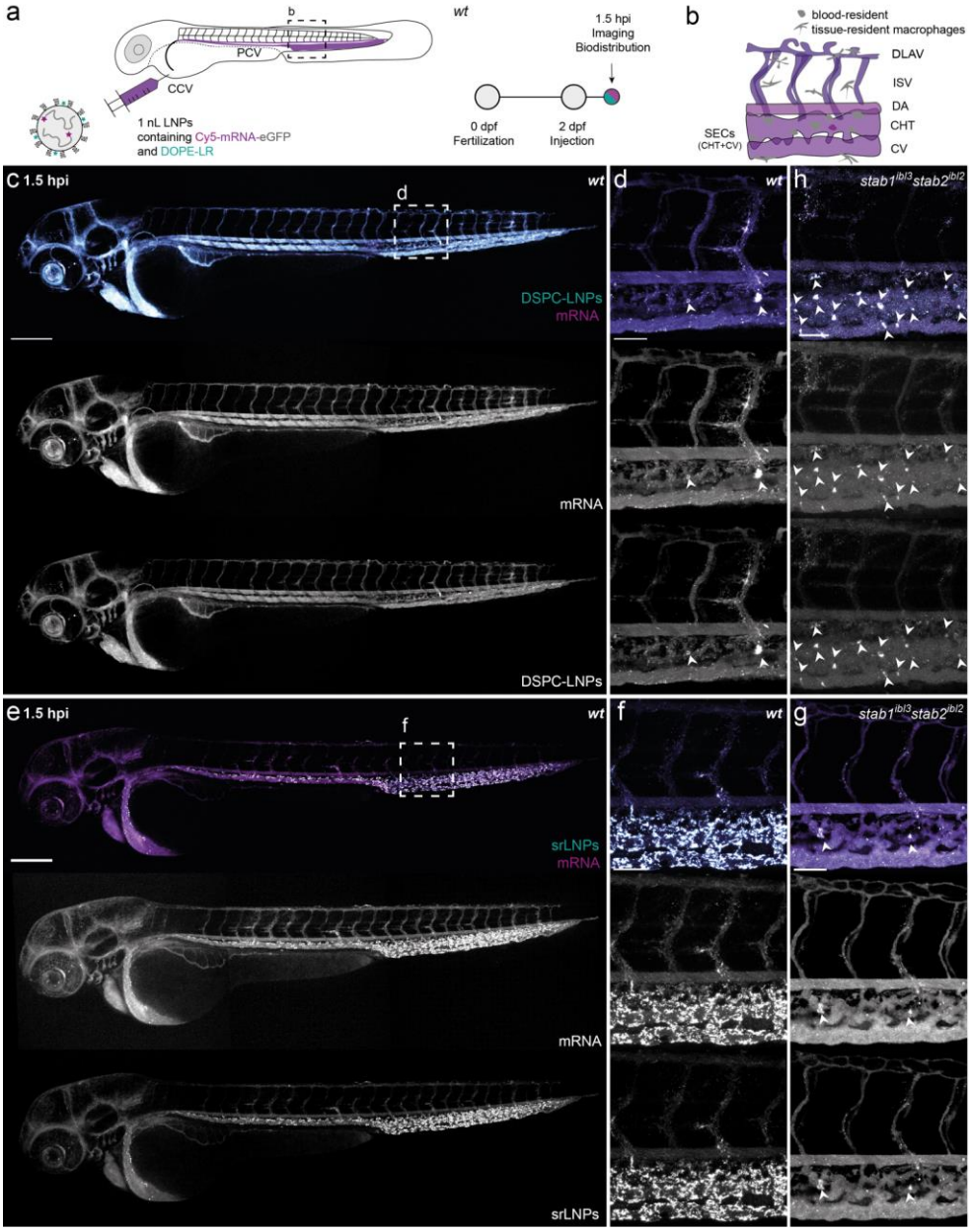

Figure 2. Biodistribution of DSPC-LNPs and srLNPs in two-day old embryonic zebrafish at 1.5 hpi. (**a**) Schematic showing the site of LNP injection (*i.v*) within embryonic zebrafish (2 dpf) and imaging timeframe. LNPs contained DOPE-LR (cyan, 0.2 mol%) as fluorescent lipid probe and Cy5-labelled eGFP mRNA (magenta) as fluorescent mRNA probe. *Injected dose*: ~10 mM lipid, ~0.2 mg/kg

mRNA. *Injection volume*: 1 nL. Major venous blood vessels: CCV – common cardinal vein; PCV – posterior cardinal vein. (**b**) Tissue level schematic of a dorsal region of the embryo containing scavenging cell types (*i.e.* SECs and blood resident macrophages). Blood vessels: DA – dorsal aorta, CHT – caudal hematopoietic tissue; CV – caudal vein; ISV – intersegmental vessel; DLAV - dorsal longitudinal anastomotic vessel. (**c,d**) Whole embryo (10x magnification) and tissue level (40x magnification) views of DSPC-LNP biodistribution within wild-type (AB/TL) embryonic zebrafish (2 dpf) at 1.5 hpi. DSPC-LNPs are mostly freely circulating, confined to, and distributed throughout, the vasculature of the embryo. Low level phagocytotic uptake within blood resident macrophages is highlighted by white arrowheads. (**e,f**) Whole embryo (10x magnification) and tissue level (40x magnification) views of srLNP biodistribution within wild-type (AB/TL) embryonic zebrafish (2 dpf) at 1.5 hpi. srLNPs are mainly associated with SECs within the PCV, CHT and CV of the embryo and are largely removed from circulation at 1.5 hpi. Phagocytotic uptake of both DSPC-LNPs and srLNPs within blood resident macrophages at 1.5 hpi was confirmed by analogous LNP injections in transgenic *mpeg*:mCherry zebrafish embryos, stably expressing mCherry within macrophages (Figure S1). (**g**) Tissue level (40x magnification) view of srLNP biodistribution within double knockout (*stab1*^{ibl3}/*stab2*^{ibl2})[51]zebrafish embryos at 1.5 hpi. Within Stabilin KOs, srLNPs are now mostly freely circulating, with low level phagocytotic uptake within blood resident macrophages highlighted by white arrowheads. (**h**) Tissue level (40x magnification) view of DSPC-LNP biodistribution within double knockout (*stab1*^{ibl3}/*stab2*^{ibl2})[51] zebrafish embryos at 1.5 hpi. Within Stabilin KOs, DSPC-LNPs remain mostly freely circulating, with low level phagocytotic uptake within blood resident macrophages highlighted by white arrowheads. Scale bars: 200 μm (whole embryo) and 50 μm (tissue level).

To assess LNP-mediated delivery of functional mRNA within the embryonic zebrafish, we switched to unlabeled eGFP mRNA (capped, **Figure 3a**), as we consistently observed low mRNA expression levels using Cy5-labeled eGFP (capped) mRNA payloads. This alteration did not significantly change the structure, surface charge or mRNA encapsulation efficiency of LNPs (see **Supporting Table 1**). At 1.5 hpi, srLNPs (~10 mM lipid, ~0.2 mg/kg mRNA) again associated with SECs and blood-resident macrophages within the PCV, CHT and CV of the embryonic zebrafish (**Figure 3b,c**). Given the >2 h timeframe for mRNA delivery, expression and maturation of eGFP,[52,53] low level green fluorescence observed at 1.5 hpi, within the yolk sac and iridophores (pigment cells) of the embryo, is attributed to embryo autofluorescence in the GFP channel.[54] However, at 24 hpi, intense eGFP fluorescence was observed specifically within SECs and blood-resident macrophages of the embryo (Figure 3d,e). This is consistent with the timing reported for eGFP-mRNA delivery and expression using analogous lipid-based delivery systems, whereby the onset of eGFP maturation and fluorescence (*in vitro*) occurs 2-7 h post-incubation and expression levels (fluorescence intensity) continually increase up to 24 h post-treatment.[52 55] Within *stab1*$^{-/-}$/*stab2*$^{-/-}$ KO embryos, srLNP-mediated eGFP expression was observed only within blood-resident

macrophages and not SECs at 24 hpi, confirming macrophage uptake of srLNPs, as for other anionic nanoparticles, is not dependent on Stabilin receptors (**Figure S3**).

For srLNPs, the resulting eGFP expression pattern mirrored srLNP biodistribution at 1.5 hpi (**Figure 2e,f**), confirming successful transport, uptake and cytosolic delivery of functional mRNA within these cells. This is particularly remarkable given SECs have one of the highest endo/lysosomal activities of any cell type in the body,[28,33] and are therefore primed to degrade fragile RNA molecules. Endosomal escape and cytosolic delivery of RNA is widely recognized as one of the major obstacles in the development of effective RNA therapies,[56] with <2% of internalized siRNA (complexed within LNPs based on the lipid composition of Onpattro®) reaching the cytoplasm of HeLa cells (*in vitro*) and hepatocytes (*in vivo*).[57,58] Indeed, the acute extent of mRNA degradation within SECs (as well as potential mRNA degradation in circulation), was confirmed by injection (*i.v.*) of free eGFP-mRNA (capped; both Cy5-labeled and unlabeled) within the zebrafish embryo. This resulted in no significant expression of eGFP within SECs at 24 hpi despite extensive accumulation within these cells at 1.5 hpi, presumably *via* scavenger receptor-mediated uptake of circulating, polyanionic RNA (**Figure S4**).[59]

In the case of DSPC-LNP (~10 mM lipid, ~0.2 mg/kg mRNA) mediated mRNA delivery, widespread eGFP fluorescence was observed throughout the embryo at 24 hpi (**Figure S5**). Combined with the evident lack of cellular accumulation at 1.5 hpi (**Figure 2c,d**), this indicates low-level, non-specific cellular uptake of LNPs based on the lipid composition of Onpattro®, with concurrent mRNA expression across a broad range of cell types, including SECs and blood-resident macrophages. Importantly, however, the liver of the embryonic zebrafish has yet to fully develop at 2 dpf.[60,61] To assess *in vivo* LNP interactions with a functional liver, and potentially corroborate reported hepatocyte targeting of Onpattro® in mammals, we therefore switched to LNP injections in older zebrafish embryos.

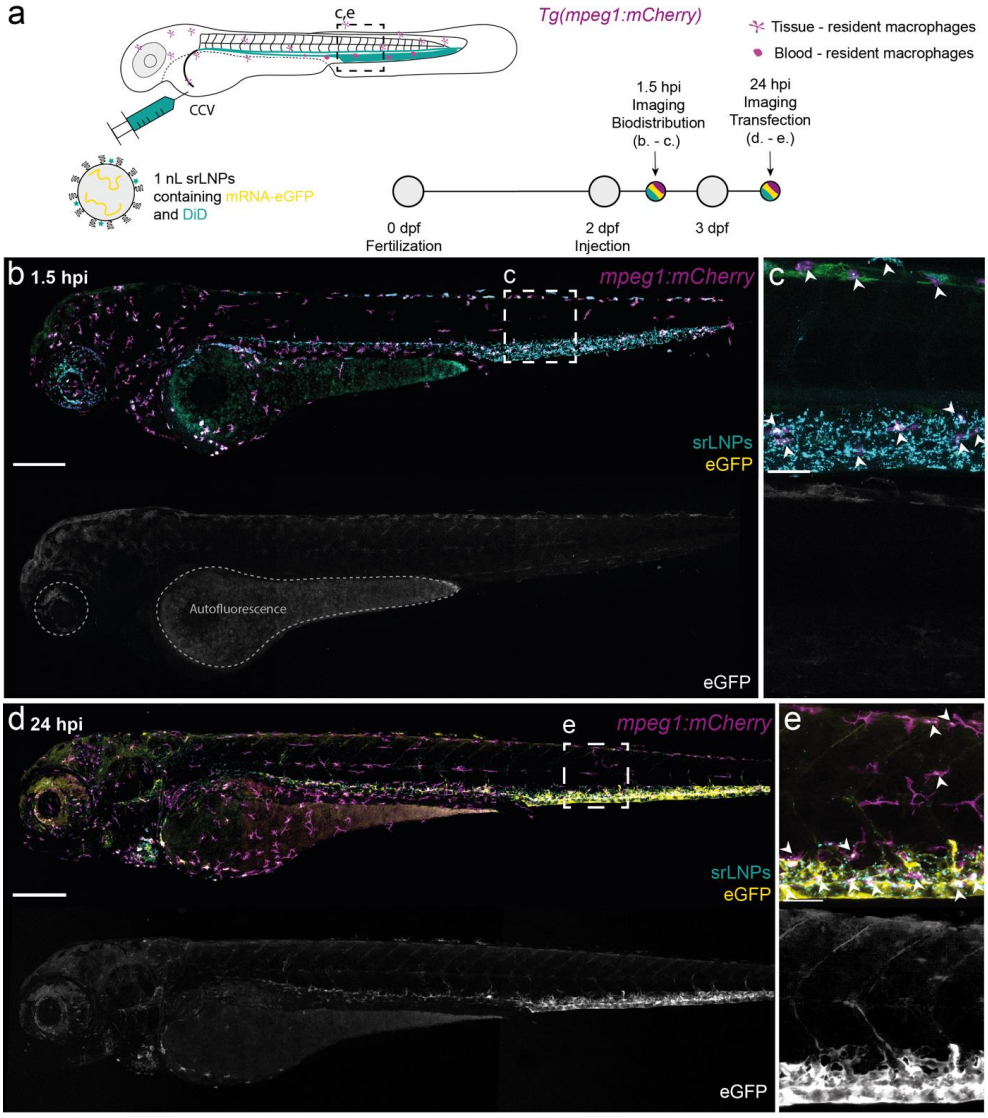

Figure 3. srLNP biodistribution, eGFP-mRNA delivery and eGFP expression within *mpeg1*:mCherry transgenic zebrafish embryos at 1.5 and 24 hpi. (**a**) Schematic showing the site of srLNP injection (*i.v.*) within embryonic zebrafish (2 dpf) and imaging timeframe. srLNPs contained DiD (Cy5, 0.1 mol%) as fluorescent lipid probe and unlabeled, eGFP mRNA (capped) payload. *Injected dose*: ~10 mM lipid, ~0.2 mg/kg mRNA. *Injection volume*: 1 nL. Transgenic Tg(*mpeg1*:mCherry) zebrafish embryos stably express mCherry (magenta) within all macrophages. (**b,c**) Whole embryo (10x magnification) and tissue level (40x magnification) views of srLNP biodistribution and eGFP

expression within the embryonic zebrafish at 1.5 hpi. srLNPs were associated with SECs and blood resident macrophages (white arrowheads) within the PCV, CHT and CV of the embryo. Low level autofluorescence in the GFP channel is highlighted within the yolk sac and pigment cells of the embryo. (**d,e**) Whole embryo and tissue level views of srLNP biodistribution and eGFP expression within the embryonic zebrafish at 24 hpi. At this timepoint, srLNPs remain associated with SECs and blood resident macrophages (white arrowheads) within the PCV, CHT and CV of the embryo. However, intense eGFP expression was now observed specifically within the PCV, CHT and CV confirming successful cytosolic delivery and translation of functional eGFP mRNA within SECs and blood resident macrophages. Scale bars: 200 µm (whole embryo) and 50 µm (tissue level).

From approximately 55 hours post-fertilisation (hpf), the liver of the embryonic zebrafish undergoes a dramatic growth phase. New intrahepatic blood vessels are formed, with blood circulation detected from 72 hpf,[62] and the localised expression of key hepatocyte markers, including transferrin (Tf)[63] and liver fatty acid binding protein (L-FABP),[64] evidently marking maturation of functional hepatoctyes. During this growth phase, anatomical features characteristic of the mammalian liver, and important for the correct processing of lipid nanoparticles, also emerge, including a Space of Disse,[65] the likely presence of a fenestrated endothelium[66] and a functional biliary network (connected to the blood vasculature *via* hepatocytes).[60] These features, combined with a conserved repertoire of lipid transport proteins,[67,68] including apoE, and lipoprotein receptors, including LDLR,[69,70] suggest older (> 72 hpf) zebrafish embryos may offer an attractive *in vivo* model to assess endogenous lipid transport mechanisms, including lipid processing disorders,[71] and probe their prospective role in the fate of LNPs within mammals.

To verify liver development timings and to assess the suitability of the embryonic zebrafish as a predictive *in vivo* model for hepatocyte targeting of nanomedicines, non-PEGylated liposomes (~100 nm), co-formulated with cholesterol-conjugated, human apoE target peptides (Chol-NH-apoE peptide, 5 mol%, see supporting information for synthesis and characterisation), were administered within 3 and 4 day old zebrafish embryos (*L-FABP*:eGFP transgenic line, stably expressing L-FABP-eGFP fusion proteins within hepatocytes) (**Figure 4a,b**). Nanoparticle/macromolecule-conjugated, apoE target peptides (*amino acid sequence*: $(LRKLRKRLL)_2$; tandem-repeat LDLR target sequence (residues 159-167) of human apoE) have been previously shown to interact with LDLr, as well as the low-density lipoprotein receptor-related proteins, LRP1 and LRP2.[72–74] Following liposome (~5 mM) administration within a zebrafish embryo at 3 dpf (74 hpf), no significant fluorescence (eGFP) was observed in the region of the developing liver and apoE-targeted liposomes remained mostly freely circulating (**Figure 4c**). At 4 dpf (98 hpf), however, the liver of the embryo, delineated by transgenic eGFP-L-FABP fluorescence, was

evidently present and *i.v.* adminstered apoE-targeted liposomes now clearly accumulated within the liver vasculature (**Figure 4d-f**). Interestingly, we observed no significant colocalisation of apoE-targeted liposomes and hepatocytes within the liver at 1.5 hpi. This may be due to liposome accumulation within the Space of Disse, as has been described for the hepatic clearance of albumin within embryonic zebrafish at 12 dpf.[66] Crucially, however, unmodified DOPC liposomes did not accumulate within the embryonic liver of either a three- or four-day old embryo, confirming liver accumulation of apoE-targeted liposomes within a four-day old zebrafish embryo was exclusively mediated by apoE target peptides (**Figure S6**). Overall, these observations confirm apoE-mediated targeting of nanoparticles to the liver of the zebrafish embryo is possible from 4 dpf.

After verification of apoE-mediated liver targeting of liposomes, we next injected DSPC-LNPs (~10 mM, ~0.2 mg/kg mRNA, **Figure 5a-e**; ~30 mM, ~0.6 mg/kg mRNA, **Figure 5f-i**) and srLNPs (~30 mM, ~0.6 mg/kg mRNA, **Figure S7**) in four day old zebrafish embryos. In the case of srLNPs, particles remained largely associated within the PCV, CV and CHT of the 4 day old embryo at 1.5 hpi, and exogenous eGFP expression was primarily restricted within ECs of these venous blood vessels at 24 hpi. No significant srLNP accumulation (at 1.5 hpi) or mRNA expression (at 24 hpi) was observed within the liver, confirming RES targeting of srLNPs remains predominant even in the presence of a functional liver.

In the case of DSPC-LNPs (~10 mM), no signficant LNP liver accumulation (1.5 hpi), nor liver specific eGFP expression (24 hpi), was observed within the four day old embryo (**Figure 5b-e**). Increasing the dose threefold (~30 mM), however, did result in significant eGFP expression throughout the entire embryo, including the liver (**Figure 5f-i**). Again, with no apparent liver targeting of DSPC-LNPs at 1.5 hpi, these observations indicate that DSPC-LNPs ineffectively target functional hepatocytes of the embryonic zebrafish *via* endogenous apoE-mediated lipid trafficking pathways. Instead, DSPC-LNPs are liable to low-level non-specific uptake and mRNA delivery and expression across a wide range of cell types, as has been previously observed.[75]

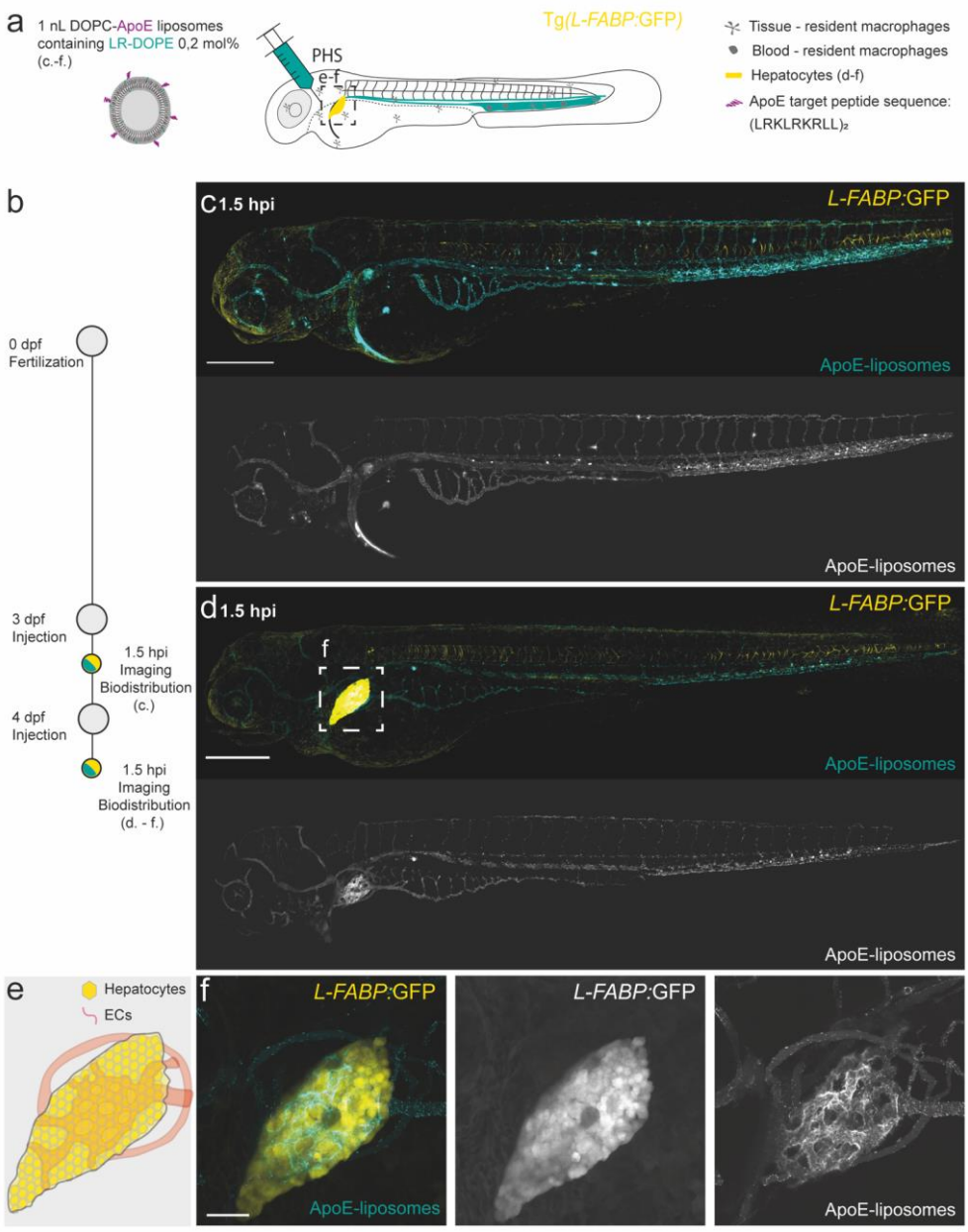

Figure 4. Biodistribution of apoE-targeted liposomes in three- and four-day old zebrafish embryos. (**a**) Schematic showing the site of apoE-targeted liposome injection (*i.v.*) within embryonic zebrafish (at 3 and 4 dpf). Liposomes contained 0.2 mol% DOPE-lissamine rhodamine as fluorescent lipid probe (cyan). *Injected dose*: ~5 mM lipid, ~5 mol% ApoE target ligand (*amino acid primary sequence*:

(LRKLRKRLL)$_2$), *Injection volume*: 1 nL. Transgenic *Tg*(*LFABP*:eGFP) zebrafish embryos stably express eGFP (yellow) within hepatocytes. PHS – primary head sinus. (**b**) Injection and imaging timeframe. (**c,d**) Whole embryo (10x magnification) views of apoE-targeted liposome biodistribution within (**c**) three- and (**d**) four-day old embryonic zebrafish at 1.5 hpi. (**e**) Tissue level schematic of the embryonic liver at 4 dpf. (**f**) Tissue level (40x magnification) views of apoE-targeted liposome biodistribution within the liver of a four-day old embryo. Within the embryonic liver, liposomes appear predominantly associated with ECs and not hepatocytes. Scale bars: 200 µm (whole embryo) and 50 µm (tissue level).

Next, we validated LNP biodistribution and LNP-mediated mRNA expression patterns in mice. In particular, we focused on cell-specific LNP distribution and mRNA expression within the murine liver, the largest RES organ in mammals. For all mouse experiments, LNP-mRNA formulations were injected (*i.v.*) in 8–10-week-old C57BL/6 mice (**Figure 6a**). To assess LNP distribution and functional mRNA delivery within individual hepatic and non-hepatic (*i.e.*, spleen) RES cell types, mice were anesthetized, a trans-cardiac collagenase perfusion performed, (parenchymal and non-parenchymal hepatic) cells were separated and individual cell types detected using cell-specific antibodies (**Figure S8** for representative flow cytometry density plots). To monitor LNP biodistribution across RES cell types and tissues, LNP-mRNA formulations, containing a non-exchangeable, fluorescent lipid probe (DiD, 0.5 mol%), were administered (**Figure 6b**). At 2 hpi, for both DSPC-LNPs and srLNPs (42.75 mg/kg total lipid), we observed striking LNP accumulation within mouse liver cell types (**Figure 6c**) compared to those of the spleen (**Figure S9**) which, although smaller than the liver, is a highly efficient unit of the mononuclear phagocyte system.[76] Notably, both LNP formulations distributed to all individually isolated hepatic cell types, as has previously been described for LNP formulations based on Onpattro®.[77,78] However, srLNPs demonstrated significantly enhanced uptake ($P < 0.001$) within all liver cell types relative to DSPC-LNPs (**Figure 6d**). This confirmed that incorporating anionic DSPG into LNP-mRNA delivery systems both enhances liver tropism in general and leads to a significant shift towards LNP targeting and cellular uptake within hepatic RES cell types.

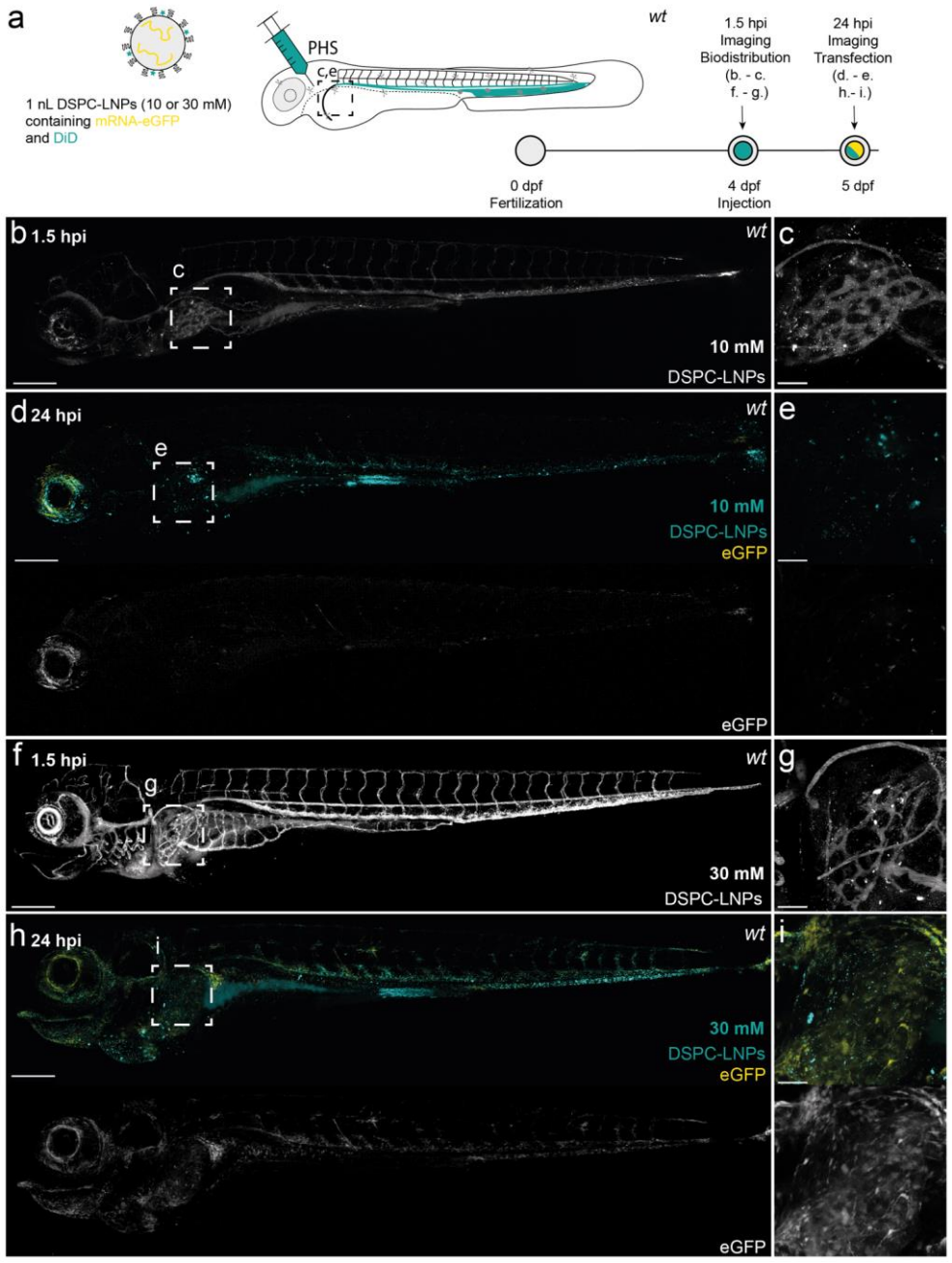

Figure 5. DSPC-LNP (10 and 30 mM) biodistribution and mRNA expression within, four-day old, wildtype (AB/TL) embryonic zebrafish. (**a**) Schematic showing the site of DSPC-LNP injection (*i.v.*) within embryonic zebrafish (4 dpf). DSPC-LNPs contained DiD (0.1 mol%) as fluorescent lipid probe

and unlabeled, eGFP mRNA (capped) payload. Injection and imaging timeframe. *Injection volume*: 1 nL. PHS – primary head sinus (**b,c**) Whole embryo (10x magnification) and tissue level (liver region, 40x magnification) views of DSPC-LNP biodistribution at 1.5 hpi. *Injected dose*: ~10 mM lipid, ~0.2 mg/kg mRNA. LNPs were mostly freely circulating with no significant accumulation in the liver at 1.5 hpi. Intense fluorescent punctae within the liver region are likely due to macrophage uptake. (**d,e**) Whole embryo (10x magnification) and tissue level (liver region, 40x magnification) views of eGFP expression at 24 hpi. (**f,g**) Whole embryo (10x magnification) and tissue level (liver region, 40x magnification) views of DSPC-LNP biodistribution at 1.5 hpi. *Injected dose*: ~30 mM lipid, ~0.6 mg/kg mRNA. At both dosages, LNPs were mostly freely circulating with no significant accumulation in the liver observed at 1.5 hpi. Intense fluorescent punctae within the liver region are likely due to macrophage LNP uptake. (**h,i**) Whole embryo (10x magnification) and tissue level (liver region, 40x magnification) views of eGFP expression at 24 hpi. At 30 mM dosage, low level eGFP fluorescence is observed throughout the embryo, including within the liver region. Confocal microscope settings were identical across all experiments. Scale bars: 200 µm (whole embryo) and 50 µm (tissue level).

To confirm functional mRNA delivery to hepatic RES cells, LNPs entrapping capped mCherry-mRNA (0.25 mg/kg mRNA) were administered (**Figure 6e**). This dosage is in line with other systemically administered LNP-mRNA therapies, including those currently in clinical trials (*e.g.* NCT03829384).[79] Following organ isolation and cell separation at 24 hpi, both srLNPs and DSPC-LNPs yielded comparable mCherry expression in hepatocytes, as well as within splenic RES cell types (**Figure 6f**, **Figure S9**). In contrast, srLNPs yielded significantly enhanced mRNA delivery to hepatic RES cell types relative to DSPC-LNPs ($P < 0.001$) (**Figure 6g**). Importantly, for both srLNPs and DSPC-LNPs, absolute mCherry expression levels within hepatocytes were significantly higher than other cell types analyzed. This apparent disparity between LNP cellular targeting and functional mRNA expression could be explained by the adverse (high) endosomal activity within LSECs and KCs (leading to significant mRNA degradation despite extensive LNP internalization), combined with the high translational efficiency of hepatocytes (leading to significant mRNA expression despite comparably low LNP internalization).[80] Interestingly, a four-fold dosage increase (1 mg/kg mRNA) resulted in significantly enhanced absolute mRNA expression within LSECs relative to hepatocytes and KCs, potentially indicative of dynamic competition between these cell types in recognizing and internalizing circulating LNPs (**Figure S10**). Since no LNP technology has yet demonstrated exclusive targeting to a single cell type *in vivo*, these findings reaffirm the importance of considering not only LNP biodistribution but also cellular physiology (both in the healthy and diseased state) in the development of new LNP technologies with novel targeting function. Overall, our data confirm that charge modifications to an LNP surface leads to preferential targeting of the hepatic RES and a significant increase in the absolute levels of functional mRNA expression within these cell types.

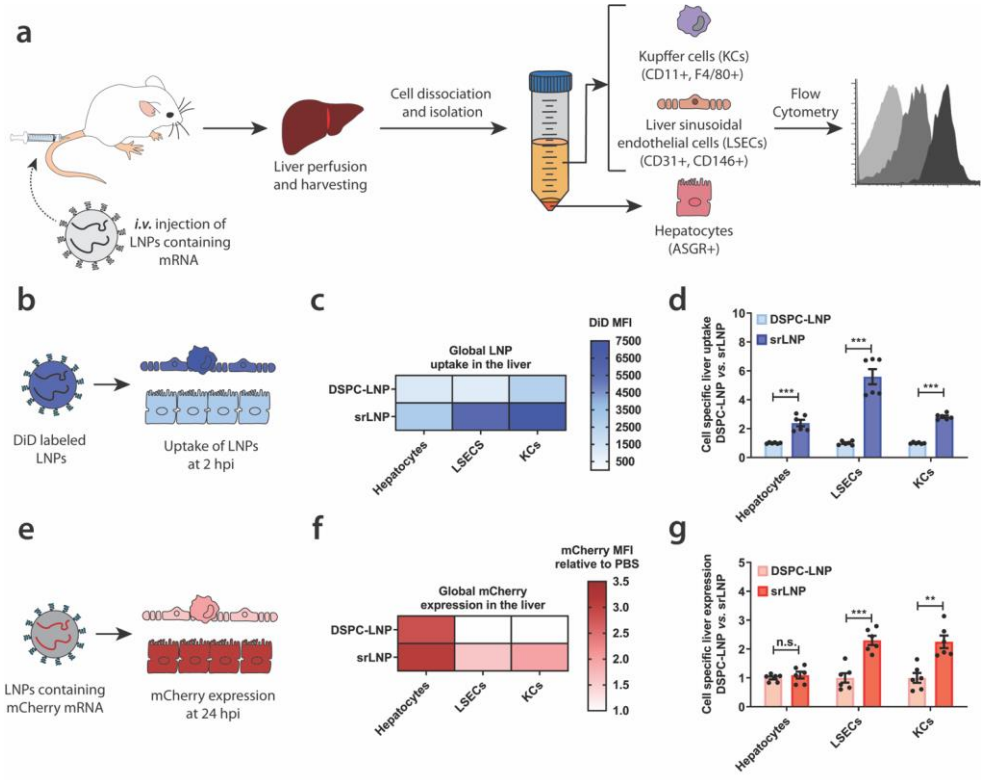

Figure 6. LNP uptake and functional mRNA delivery within different hepatic cell types. (**a**) Schematic illustrating the procedure to isolate different hepatic cell types and determine LNP-mRNA targeting and functional mRNA delivery. Following intravenous LNP-mRNA injection (*i.v*) the liver was perfused with collagenase IV, hepatic cells were isolated and stained with specific antibodies, and flow cytometry was used to analyze LNP uptake and gene expression. Specific antibody markers used to uniquely identify hepatocytes, LSECs and KCs, respectively, are defined in parentheses. (**b**) For intrahepatic biodistribution studies, LNPs contained DiD (0.5 mol%) as fluorescent lipid probe. Cellular uptake of DSPC-LNP and srLNP was assessed following mouse sacrifice at 2 hpi. *Injected dose*: 42.75 mg/kg total lipid. (**c**) Heatmap of global LNP uptake in the liver determined by absolute DiD fluorescence. srLNP demonstrate significantly enhanced LNP uptake within all hepatic cell types, and significant re-direction to hepatic RES compared to DSPC-LNPs. (**d**) Cell specific liver uptake normalized to DSPC-LNP for each cell type. (**e**) For gene expression experiments, LNPs contained capped, mCherry-mRNA. Functional mRNA delivery was assessed based on mCherry fluorescence levels following mouse sacrifice at 24 hpi. (**f**) Heatmap of mCherry expression in different liver cell types following functional mRNA delivery using DSPC-LNP and srLNP. *Injected dose*: 0.25 mg/kg mRNA. (**g**) Cell specific mCherry expression normalized to DSPC-LNP for each cell type. In all cases, n = 6 represents 3 separate liver tissue samples from 2 mice sorted

into individual cell types. Bars and error bars in d and g represent mean ± s.e.m. The data was normalized to the average uptake and expression of DSPC-LNPs within each cell type. Statistical significance was evaluated using a two-tailed unpaired Student's t-test. n.s. = not significant, ** $p < 0.01$, *** $p < 0.001$. Exact P values for d: Hepatocytes P= 0.00011, LSECs P= $1.12*10^{-5}$, KCs P= $3.62*10^{-9}$. Exact P values for g: Hepatocytes P= 0.464, LSECs P= 0.00064, KCs P= 0.0023.

3.3 Discussion

Based on a robust understanding of the nano-bio interactions involved,[36] we have rationally designed an LNP platform capable of preferentially targeting the hepatic RES and enhanced mRNA expression within hepatic RES cell types. Given the importance of the hepatic RES in establishing and maintaining the liver microenvironment, as well as in the pathogenesis of many liver-specific and systemic diseases,[26,81] including (auto)immune diseases,[35] we believe anionic LNP formulations can form the basis of future RNA gene therapies against acquired and inherited diseases in which hepatic RES cell types play a central role.[34] Here, it is important to recognize the extensive refinement of both ionizable[82–84] and sterol lipid components of LNPs[50] (primarily to promote endosomal rupture/escape and cytosolic RNA delivery), as well as chemical modifications to RNA (to improve stability, translation proficiency and reduce immunogenicity), that have already been made.[85–87] These optimized reagents can improve transfection efficiency >10-fold, compared to LNPs based on the lipid composition of Onpattro®,[82,83] meaning anionic, srLNP formulations could, if necessary, be simply retrofitted to widen any potential therapeutic window.

Existing LNP technologies that have demonstrated preferential RNA delivery to non-parenchymal hepatic cell types and/or non-hepatic cells have all been discovered through bottom-up empirical screens. These discoveries have not revealed the biological mechanisms underpinning any observed cellular preference. Preferential delivery of mRNA to liver ECs has, for example, been achieved through the replacement of cholesterol with either cholesteryl oleate or oxidized cholesterol components.[18,19] While these observations may conform to a charge-dependent, Stabilin-mediated mechanism of uptake within LSECs, as has been observed for both OxLDL and AcLDL,[27,88] in the absence of reported zeta potentials, and given both sterol reagents likely predominate within the LNP core, this could equally point to an alternative mechanism of LNP recognition and uptake within hepatic RES cell types. Alternatively, exclusive LNP-mediated RNA delivery to the spleen has been achieved by adding the anionic phospholipid, 18PA (up to 30 mol%), to the lipid composition of Onpattro®.[89] Assuming the measured surface charge of these formulations is also anionic (and given srLNPs showed negligible accumulation within the spleen), this suggests simply rendering an LNP anionic does not necessarily guarantee preferential

uptake within hepatic RES cell types. Overall, these studies highlight the complex interplay between LNP compositional makeup, biophysical properties and structure, and the implications these factors have in determining the *in vivo* fate of an LNP. Given the exploitable chemical space of an LNP is vast, the targeting of innate immune cells and hepatocytes – primed to recognize and internalize waste and/or pathogenic (lipid) particles – may therefore reflect only a small, easily accessible fraction of preferential LNP cellular tropisms. Consequently, the discovery of new LNP platforms capable of preferential cellular targeting beyond RES cells and/or hepatocytes would undoubtedly benefit from a more focused and informed screening approach.

To this end, the elucidation and exploitation of fundamental mechanisms dictating both endogenous and exogenous lipid particle fate *in vivo* can focus and direct empirical screens for new LNP formulations. It is worth emphasizing that all cells rely, to some extent, on systemic lipid transport to ensure correct function. We therefore believe the embryonic zebrafish is a powerful addition to the discovery pipeline for new LNP technologies,[37] both as a screening platform and as a tool to probe fundamental biology. As a screening and optimization tool, zebrafish embryos permit real-time, *in vivo* visualization of total LNP injected doses at cellular resolution. Furthermore, with a conserved repertoire of RES cell types, hepatocytes, soluble lipid transport proteins and receptors, the data acquired within these animals can offer accurate qualitative predictions of cell specific LNP recognition and uptake within key mammalian RES organs. Furthermore, up to 5 dpf, the number of different LNP formulations that can be screened is limited only by practical considerations of time and capacity. As a fundamental tool to elucidate biological mechanisms underpinning LNP transport and RNA delivery, the short generational time of the zebrafish (approx. 3 months), the extensive repertoire of established (fluorescent) transgenic lines and antibodies,[90,91] optimized techniques for genetic manipulation (including CRISPR/Cas)[92] and advanced imaging techniques, enable key nano-bio interactions underpinning LNP fate *in vivo* to be rapidly assessed and confirmed.

In conclusion, the widespread evaluation of LNP-based mRNA therapies as potential prophylactic vaccines,[93,94] notably against COVID-19,[95–98] has provided further proof of the broad therapeutic potential of these platform mRNA technologies. Despite the obvious differences in therapeutic target, mode of action and injection site, however, all LNP-mRNA vaccine candidates to date closely resemble the lipid composition of Onpattro®. In particular, LNP surface lipids (*i.e.* "helper" phospholipids and PEG lipids), cholesterol content and overall lipid composition are strikingly similar between different clinical formulations. Based on our observations, these vaccines can be expected to elicit broad mRNA expression profiles. Indeed, following intramuscular (*i.m.*) injection of an LNP-

mRNA COVID-19 vaccine candidate, mRNA (coding for the receptor binding domain (RBD) of SARS-CoV-2) expression was observed across a broad spectrum of cell types, including intramuscular and hepatic immune cells, as well as hepatocytes.[95] However, while the ability to leverage a wide array of cell types to produce a therapeutic protein may be safe and effective as a systemic secreted therapy (*i.e.* suitable for vaccine application), the lack of LNP designs capable of preferentially delivering RNA to specific diseased cells and tissues in the body remains a major limitation. For although cell specificity of LNP-mRNA systems can be enhanced, for example, through microRNA regulation of mRNA expression,[99] these technologies still rely on LNPs reaching and delivering functional mRNA within target cells at therapeutically relevant doses. To this end, we believe a top-down approach to LNP discovery, based on pre-existing knowledge of the nano-bio interactions, can guide and focus (high throughput) empirical screening. This will surely expedite the necessary discovery of new LNP designs with inherent tropisms for specific and varied cell types.

3.4 References

1. Delivering the promise of RNA therapeutics. *Nat. Med.* **25**, 1321 (2019).
2. Dammes, N. & Peer, D. Paving the Road for RNA Therapeutics. *Trends Pharmacol. Sci.* **41**, 755–775 (2020).
3. Yin, H. *et al.* Non-viral vectors for gene-based therapy. *Nat. Rev. Genet.* **15**, 541–555 (2014).
4. Cullis, P. R. & Hope, M. J. Lipid Nanoparticle Systems for Enabling Gene Therapies. *Mol. Ther.* **25**, 1467–1475 (2017).
5. Kulkarni, J. A., Witzigmann, D., Chen, S., Cullis, P. R. & van der Meel, R. Lipid Nanoparticle Technology for Clinical Translation of siRNA Therapeutics. *Acc. Chem. Res.* **52**, 2435–2444 (2019).
6. Akinc, A. *et al.* The Onpattro story and the clinical translation of nanomedicines containing nucleic acid-based drugs. *Nat. Nanotechnol.* **14**, 1084–1087 (2019).
7. Adams, D. *et al.* Patisiran, an RNAi therapeutic, for hereditary transthyretin amyloidosis. *N. Engl. J. Med.* **379**, 11–21 (2018).
8. Kumar, V. *et al.* Shielding of Lipid Nanoparticles for siRNA Delivery: Impact on Physicochemical Properties, Cytokine Induction, and Efficacy. *Mol. Ther. Nucleic Acids* **3**, e210 (2014).
9. Mui, B. L. *et al.* Influence of Polyethylene Glycol Lipid Desorption Rates on Pharmacokinetics and Pharmacodynamics of siRNA Lipid Nanoparticles. *Mol. Ther. Nucleic Acids* **2**, e139 (2013).
10. Akinc, A. *et al.* Targeted delivery of RNAi therapeutics with endogenous and exogenous ligand-based mechanisms. *Mol. Ther.* **18**, 1357–1364 (2010).
11. Nguyen, J. & Szoka, F. C. Nucleic acid delivery: the missing pieces of the puzzle? *Acc. Chem. Res.* **45**, 1153–1162 (2012).
12. Sato, Y. *et al.* Highly specific delivery of siRNA to hepatocytes circumvents endothelial cell-mediated lipid nanoparticle-associated toxicity leading to the safe and efficacious decrease in the hepatitis B virus. *J. Control. Release* **266**, 216–225 (2017).

13. DeRosa, F. *et al.* Therapeutic efficacy in a hemophilia B model using a biosynthetic mRNA liver depot system. *Gene Ther.* **23**, 699–707 (2016).
14. Ramaswamy, S. *et al.* Systemic delivery of factor IX messenger RNA for protein replacement therapy. *Proc. Natl. Acad. Sci. U. S. A.* **114**, E1941–E1950 (2017).
15. Chen, S. *et al.* Development of lipid nanoparticle formulations of siRNA for hepatocyte gene silencing following subcutaneous administration. *J. Control. Release* **196**, 106–112 (2014).
16. Sago, C. D. *et al.* Nanoparticles That Deliver RNA to Bone Marrow Identified by in Vivo Directed Evolution. *J. Am. Chem. Soc.* **140**, 17095–17105 (2018).
17. Lokugamage, M. P., Sago, C. D., Gan, Z., Krupczak, B. R. & Dahlman, J. E. Constrained Nanoparticles Deliver siRNA and sgRNA to T Cells In Vivo without Targeting Ligands. *Adv. Mater.* **31**, 1902251 (2019).
18. Paunovska, K. *et al.* Analyzing 2,000 in vivo Drug Delivery Data Points Reveals Cholesterol Structure Impacts Nanoparticle Delivery. *ACS Nano* **12**, 8341–8349 (2018).
19. Paunovska, K. *et al.* Nanoparticles Containing Oxidized Cholesterol Deliver mRNA to the Liver Microenvironment at Clinically Relevant Doses. *Adv. Mater.* **31**, e1807748 (2019).
20. Witzigmann, D., Hak, S. & van der Meel, R. Translating nanomedicines: Thinking beyond materials? A young investigator's reply to 'The Novelty Bubble'. *J. Control. Release* **290**, 138–140 (2018).
21. Trefts, E., Gannon, M. & Wasserman, D. H. The liver. *Curr. Biol.* **27**, R1147–R1151 (2017).
22. Wisse, E. An electron microscopic study of the fenestrated endothelial lining of rat liver sinusoids. *J. Ultrastruct. Res.* **31**, 125–150 (1970).
23. Braet, F. & Wisse, E. Structural and functional aspects of liver sinusoidal endothelial cell fenestrae: a review. *Comp. Hepatol.* **1**, 1–17 (2002).
24. Smedsrød, B., Pertoft, H., Gustafson, S. & Laurent, T. C. Scavenger functions of the liver endothelial cell. *Biochem. J.* **266**, 313–327 (1990).
25. Sørensen, K. K., Simon-Santamaria, J., McCuskey, R. S. & Smedsrød, B. Liver sinusoidal endothelial cells. *Compr. Physiol.* **5**, 1751–1774 (2015).
26. Poisson, J. *et al.* Liver sinusoidal endothelial cells: Physiology and role in liver diseases. *J. Hepatol.* **66**, 212–227 (2017).
27. Li, R. *et al.* Role of liver sinusoidal endothelial cells and stabilins in elimination of oxidized low-density lipoproteins. *Am. J. Physiol. Gastrointest. Liver Physiol.* **300**, G71–G81 (2010).
28. Smedsrød, B. Clearance function of scavenger endothelial cells. *Comp. Hepatol.* **3**, S22 (2004).
29. Ganesan, L. P. *et al.* Rapid and Efficient Clearance of Blood-borne Virus by Liver Sinusoidal Endothelium. *PLOS Pathog.* **7**, e1002281 (2011).
30. Mates, J. M. *et al.* Mouse Liver Sinusoidal Endothelium Eliminates HIV-Like Particles from Blood at a Rate of 100 Million per Minute by a Second-Order Kinetic Process . *Frontiers in Immunology* **8**, 35 (2017).
31. Sørensen, K. K. *et al.* The scavenger endothelial cell: a new player in homeostasis and immunity. *Am. J. Physiol. Integr. Comp. Physiol.* **303**, R1217–R1230 (2012).
32. Schledzewski, K. *et al.* Deficiency of liver sinusoidal scavenger receptors stabilin-1 and -2 in mice causes glomerulofibrotic nephropathy via impaired hepatic clearance of noxious blood factors. *J. Clin. Invest.* **121**, 703–714 (2011).
33. McCourt, P. A. G. *et al.* The liver sinusoidal endothelial cell hyaluronan receptor and its homolog, stabilin-1 - Their roles (known and unknown) in endocytosis. *Comp. Hepatol.* **3**, S24 (2004).
34. Wilkinson, A. L., Qurashi, M. & Shetty, S. The Role of Sinusoidal Endothelial Cells in the Axis of Inflammation and Cancer Within the Liver . *Frontiers in Physiology* **11**, 990 (2020).

35. Shetty, S., Lalor, P. F. & Adams, D. H. Liver sinusoidal endothelial cells — gatekeepers of hepatic immunity. *Nat. Rev. Gastroenterol. Hepatol.* **15**, 555–567 (2018).
36. Campbell, F. *et al.* Directing Nanoparticle Biodistribution through Evasion and Exploitation of Stab2-Dependent Nanoparticle Uptake. *ACS Nano* **12**, 2138–2150 (2018).
37. Sieber, S. *et al.* Zebrafish as a preclinical in vivo screening model for nanomedicines. *Adv. Drug Deliv. Rev.* **151–152**, 152–168 (2019).
38. Seternes, T., Sørensen, K. & Smedsrød, B. Scavenger endothelial cells of vertebrates: a nonperipheral leukocyte system for high-capacity elimination of waste macromolecules. *Proc. Natl. Acad. Sci. U. S. A.* **99**, 7594–7597 (2002).
39. Smedsrod, B. Scavenger function of liver sinusoidal endothelial cells. *FASEB J.* **23**, 66.1 (2009).
40. Hayashi, Y. *et al.* Differential Nanoparticle Sequestration by Macrophages and Scavenger Endothelial Cells Visualized in Vivo in Real-Time and at Ultrastructural Resolution. *ACS Nano* **14**, 1665–1681 (2020).
41. Arteta, M. Y. *et al.* Successful reprogramming of cellular protein production through mRNA delivered by functionalized lipid nanoparticles. *Proc. Natl. Acad. Sci. U. S. A.* **115**, E3351–E3360 (2018).
42. Yamamoto, T. & Ryan, R. O. Anionic phospholipids inhibit apolipoprotein E—Low-density lipoprotein receptor interactions. *Biochem. Biophys. Res. Commun.* **354**, 820–824 (2007).
43. Evers, M. J. W. *et al.* State-of-the-Art Design and Rapid-Mixing Production Techniques of Lipid Nanoparticles for Nucleic Acid Delivery. *Small Methods* **2**, 1700375 (2018).
44. Kulkarni, J. A., Witzigmann, D., Leung, J., Tam, Y. Y. C. & Cullis, P. R. On the role of helper lipids in lipid nanoparticle formulations of siRNA. *Nanoscale* **11**, 21733–21739 (2019).
45. Kulkarni, J. A. *et al.* On The Formation and Morphology of Lipid Nanoparticles Containing Ionizable Cationic Lipids and siRNA. *ACS Nano* **12**, 4787–4795 (2018).
46. Leung, A. K. K. *et al.* Lipid nanoparticles containing siRNA synthesized by microfluidic mixing exhibit an electron-dense nanostructured core. *J. Phys. Chem. C* **116**, 18440–18450 (2012).
47. Kulkarni, J. A. *et al.* Fusion-dependent formation of lipid nanoparticles containing macromolecular payloads. *Nanoscale* **11**, 9023–9031 (2019).
48. Crawford, R. *et al.* Analysis of lipid nanoparticles by Cryo-EM for characterizing siRNA delivery vehicles. *Int. J. Pharm.* **403**, 237–244 (2011).
49. Eygeris, Y., Patel, S., Jozic, A. & Sahay, G. Deconvoluting Lipid Nanoparticle Structure for Messenger RNA Delivery. *Nano Lett.* **20**, 4543–4549 (2020).
50. Patel, S. *et al.* Naturally-occurring cholesterol analogues in lipid nanoparticles induce polymorphic shape and enhance intracellular delivery of mRNA. *Nat. Commun.* **11**, 983 (2020).
51. Arias-Alpizar, G. *et al.* Stabilin-1 is required for the endothelial clearance of small anionic nanoparticles. *Nanomedicine Nanotechnology, Biol. Med.* **34**, 102395 (2021).
52. Reiser, A. *et al.* Correlation of mRNA delivery timing and protein expression in lipid-based transfection. *Integr. Biol.* **11**, 362–371 (2019).
53. Balleza, E., Kim, J. M. & Cluzel, P. Systematic characterization of maturation time of fluorescent proteins in living cells. *Nat. Methods* **15**, 47–51 (2018).
54. Lopes, S. *et al.* Leukocyte Tyrosine Kinase Functions in Pigment Cell Development. *PLoS Genet.* **4**, e1000026 (2008).
55. Leonhardt, C. *et al.* Single-cell mRNA transfection studies: Delivery, kinetics and statistics by numbers. *Nanomedicine Nanotechnology, Biol. Med.* **10**, 679–688 (2014).

56. Patel, S. *et al.* Brief update on endocytosis of nanomedicines. *Adv. Drug Deliv. Rev.* **144**, 90–111 (2019).
57. Gilleron, J. *et al.* Image-based analysis of lipid nanoparticle–mediated siRNA delivery, intracellular trafficking and endosomal escape. *Nat. Biotechnol.* **31**, 638–646 (2013).
58. Sahay, G. *et al.* Efficiency of siRNA delivery by lipid nanoparticles is limited by endocytic recycling. *Nat. Biotechnol.* **31**, 653–658 (2013).
59. Miller, C. M. *et al.* Stabilin-1 and Stabilin-2 are specific receptors for the cellular internalization of phosphorothioate-modified antisense oligonucleotides (ASOs) in the liver. *Nucleic Acids Res.* **44**, 2782–2794 (2016).
60. Wilkins, B. J. & Pack, M. Zebrafish models of human liver development and disease. *Compr. Physiol.* **3**, 1213–1230 (2013).
61. Wang, S., Miller, S. R., Ober, E. A. & Sadler, K. C. Making It New Again: Insight Into Liver Development, Regeneration, and Disease From Zebrafish Research. *Curr. Top. Dev. Biol.* **124**, 161–195 (2017).
62. Korzh, S. *et al.* Requirement of vasculogenesis and blood circulation in late stages of liver growth in zebrafish. *BMC Dev. Biol.* **8**, 84 (2008).
63. Mudumana, S. P., Wan, H., Singh, M., Korzh, V. & Gong, Z. Expression analyses of zebrafish transferrin, ifabp, and elastaseB mRNAs as differentiation markers for the three major endodermal organs: liver, intestine, and exocrine pancreas. *Dev. Dyn. an Off. Publ. Am. Assoc. Anat.* **230**, 165–173 (2004).
64. Her, G. M., Chiang, C.-C., Chen, W.-Y. & Wu, J.-L. In vivo studies of liver-type fatty acid binding protein (L-FABP) gene expression in liver of transgenic zebrafish (Danio rerio). *FEBS Lett.* **538**, 125–133 (2003).
65. Yin, C., Evason, K. J., Maher, J. J. & Stainier, D. Y. R. The basic helix-loop-helix transcription factor, heart and neural crest derivatives expressed transcript 2, marks hepatic stellate cells in zebrafish: analysis of stellate cell entry into the developing liver. *Hepatology* **56**, 1958–1970 (2012).
66. Cheng, D., Morsch, M., Shami, G. J., Chung, R. S. & Braet, F. Albumin uptake and distribution in the zebrafish liver as observed via correlative imaging. *Exp. Cell Res.* **374**, 162–171 (2019).
67. Otis, J. P. *et al.* Zebrafish as a model for apolipoprotein biology: comprehensive expression analysis and a role for ApoA-IV in regulating food intake. *Dis. Model. Mech.* **8**, 295–309 (2015).
68. Babin, P. J. *et al.* Both apolipoprotein E and A-I genes are present in a nonmammalian vertebrate and are highly expressed during embryonic development. *Proc. Natl. Acad. Sci.* **94**, 8622–8627 (1997).
69. Liu, C. *et al.* Modeling hypercholesterolemia and vascular lipid accumulation in LDL receptor mutant zebrafish. *J. Lipid Res.* **59**, 391–399 (2018).
70. O'Hare, E. A. *et al.* Disruption of ldlr causes increased LDL-c and vascular lipid accumulation in a zebrafish model of hypercholesterolemia. *J. Lipid Res.* **55**, 2242–2253 (2014).
71. Schlegel, A. Zebrafish Models for Dyslipidemia and Atherosclerosis Research . *Frontiers in Endocrinology* **7**, 159 (2016).
72. Wang, D. *et al.* Engineering a lysosomal enzyme with a derivative of receptor-binding domain of apoE enables delivery across the blood-brain barrier. *Proc. Natl. Acad. Sci. U. S. A.* **110**, 2999–3004 (2013).
73. Jiang, Y., Zhang, J., Meng, F. & Zhong, Z. Apolipoprotein E Peptide-Directed Chimeric Polymersomes Mediate an Ultrahigh-Efficiency Targeted Protein Therapy for Glioblastoma. *ACS Nano* **12**, 11070–11079 (2018).
74. Böckenhoff, A. *et al.* Comparison of five peptide vectors for improved brain delivery of the

lysosomal enzyme arylsulfatase A. *J. Neurosci.* **34**, 3122–3129 (2014).
75. Patton, C., Farr, G. H., An, D., Martini, P. G. V. & Maves, L. Lipid Nanoparticle Packaging Is an Effective and Nontoxic mRNA Delivery Platform in Embryonic Zebrafish. *Zebrafish* **15**, 217–227 (2018).
76. Mayer, L. D., Cullis, P. R. & Bally, M. B. Designing therapeutically optimized liposomal anticancer delivery systems: Lessons from conventional liposomes. in *Medical Applications of Liposomes* 231–257 (Elsevier Science B.V., 1998).
77. Sago, C. D., Krupczak, B. R., Lokugamage, M. P., Gan, Z. & Dahlman, J. E. Cell Subtypes Within the Liver Microenvironment Differentially Interact with Lipid Nanoparticles. *Cell. Mol. Bioeng.* **12**, 389–397 (2019).
78. Shi, B. *et al.* Biodistribution of small interfering RNA at the organ and cellular levels after lipid nanoparticle-mediated delivery. *J. Histochem. Cytochem.* **59**, 727–740 (2011).
79. Moderna Announces Positive Phase 1 Results for the First Systemic Messenger RNA Therapeutic Encoding a Secreted Protein (mRNA-1944). (2019). Available at: https://investors.modernatx.com/news-releases/news-release-details/moderna-announces-positive-phase-1-results-first-systemic. (Accessed: 21st December 2020)
80. Schulze, R. J., Schott, M. B., Casey, C. A., Tuma, P. L. & McNiven, M. A. The cell biology of the hepatocyte: A membrane trafficking machine. *J. Cell Biol.* **218**, 2096–2112 (2019).
81. Ni, Y. *et al.* Pathological process of liver sinusoidal endothelial cells in liver diseases. *World J. Gastroenterol.* **23**, 7666–7677 (2017).
82. Rietwyk, S. & Peer, D. Next-Generation Lipids in RNA Interference Therapeutics. **11**, 7572–7586 (2017).
83. Miao, L. *et al.* Delivery of mRNA vaccines with heterocyclic lipids increases anti-tumor efficacy by STING-mediated immune cell activation. *Nat. Biotechnol.* **37**, 1174–1185 (2019).
84. Hassett, K. J. *et al.* Optimization of Lipid Nanoparticles for Intramuscular Administration of mRNA Vaccines. *Mol. Ther. - Nucleic Acids* **15**, 1–11 (2019).
85. Khvorova, A. & Watts, J. K. The chemical evolution of oligonucleotide therapies of clinical utility. *Nat. Biotechnol.* **35**, 238–248 (2017).
86. Ku, S. H., Jo, S. D., Lee, Y. K., Kim, K. & Kim, S. H. Chemical and structural modifications of RNAi therapeutics. *Adv. Drug Deliv. Rev.* **104**, 16–28 (2016).
87. Shen, X. & Corey, D. R. Chemistry, mechanism and clinical status of antisense oligonucleotides and duplex RNAs. *Nucleic Acids Res.* **46**, 1584–1600 (2017).
88. De Rijke, Y. B., Biessen, E. A., Vogelezang, C. J. & van Berkel, T. J. Binding characteristics of scavenger receptors on liver endothelial and Kupffer cells for modified low-density lipoproteins. *Biochem. J.* **304**, 69–73 (1994).
89. Cheng, Q. *et al.* Selective organ targeting (SORT) nanoparticles for tissue-specific mRNA delivery and CRISPR–Cas gene editing. *Nat. Nanotechnol.* **15**, 313–320 (2020).
90. Staudt, N. *et al.* A panel of recombinant monoclonal antibodies against zebrafish neural receptors and secreted proteins suitable for wholemount immunostaining. *Biochem. Biophys. Res. Commun.* **456**, 527–533 (2015).
91. Burket, C. T. *et al.* Generation and characterization of transgenic zebrafish lines using different ubiquitous promoters. *Transgenic Res.* **17**, 265–279 (2008).
92. Varshney, G. K. *et al.* High-throughput gene targeting and phenotyping in zebrafish using CRISPR/Cas9. *Genome Res.* **25**, 1030–1042 (2015).
93. Pardi, N., Hogan, M. J., Porter, F. W. & Weissman, D. mRNA vaccines — a new era in vaccinology. *Nat. Rev. Drug Discov.* **17**, 261–279 (2018).
94. John, S. *et al.* Multi-antigenic human cytomegalovirus mRNA vaccines that elicit potent

humoral and cell-mediated immunity. *Vaccine* **36**, 1689–1699 (2018).
95. Zhang, N.-N. *et al.* A Thermostable mRNA Vaccine against COVID-19. *Cell* **182**, 1271–1283 (2020).
96. Jackson, L. A. *et al.* An mRNA Vaccine against SARS-CoV-2 — Preliminary Report. *N. Engl. J. Med.* **383**, 1920–1931 (2020).
97. McKay, P. F. *et al.* Self-amplifying RNA SARS-CoV-2 lipid nanoparticle vaccine candidate induces high neutralizing antibody titers in mice. *Nat. Commun.* **11**, 3523 (2020).
98. Lu, J. *et al.* A COVID-19 mRNA vaccine encoding SARS-CoV-2 virus-like particles induces a strong antiviral-like immune response in mice. *Cell Res.* **30**, 936–939 (2020).
99. Jain, R. *et al.* MicroRNAs Enable mRNA Therapeutics to Selectively Program Cancer Cells to Self-Destruct. *Nucleic Acid Ther.* **28**, 285–296 (2018).